Electronic Supplementary Material (ESI) for Journal of Materials Chemistry A.

Measuring Effective Stiffness of Li-ion Batteries via Acoustic Signal Processing

Wesley Chang[1,4,6,7], Robert Mohr[6,7], Andrew Kim[3,4], Abhi Raj[3,4], Greg Davies[4], Kate Denner[1], Jeung Hun Park[1,2,4,6,*], and Daniel Steingart[1,2,4,5,6,7,*]

[1]Department of Mechanical and Aerospace Engineering, [2]Department of Chemical and Biological Engineering, [3]Department of Electrical Engineering, and [4]Andlinger Center for Energy and the Environment, Princeton University, Princeton, NJ 08540 USA,

[5]Department of Earth and Environmental Engineering, [6]Department of Chemical Engineering, and [7]Columbia Electrochemical Energy Center, Columbia University, New York, NY 10027 USA

*Correspondence: dan.steingart@columbia.edu (D.S.), jeungp@princeton.edu (J.H.P.)

SUPPLEMENTARY MATERIALS

Supplementary materials contain additional information on experimental procedures, cell properties, TXM radiographs, and supporting electrochemical data.

Supplementary Movies: *Operando* bright-field transmission X-ray microscopy of 210 mAh $LiCoO_2$/graphite pouch cells, coupled with acoustic-electrochemical-mechanical analysis. Pouch cells were tested at rates of 1C (Movie M1), 2C (Movie M2), and 3C (Movie M3). All movies are playing at 100x real time. Note that the voltage/current profiles for every 5th cycle are not properly shown due to a potentiostat data saving error.

Cell Property Information:

Chemical composition of the commercial 210 mAh $LiCoO_2$/graphite pouch cells are listed in Table S1, from the manufacturer specification sheet.

Table S1. Chemical Composition.

Chemical Name	Content (wt%)	CAS Index No.
Lithium cobalt oxide	50	12190-79-3
Graphite	10	7782-42-5
Polypropylene	5	9003-07-0
PVDF	2	24937-79-9
Polyethylene	5	9002-88-4
Carboxymethylcellulose	0.5	9004-32-4
Lithium hexafluorophosphate	5	21324-40-3
Ethylene carbonate	5	96-49-1
Dimethyl carbonate	5	616-38-6
Nickel	2.5	7440-02-0
Copper	5	7440-50-8
Aluminum	5	7429-90-5

As depicted in Figure 1, each transducer (transmitting and receiving) is held in mechanical contact with the pouch cell via precision compression springs. From the TXM thickness measurements, it is possible to calculate the displacement of the transducer springs assuming that the cell holder is rigid and an unchanging spring constant within the displacement regime. Caliper compression measurements of the holder indicate that the holder is rigid enough to remain incompressible within the duration of the cycling studies. The maximum pouch cell displacement observed over a complete experiment was 0.7 mm, which is significantly less than the loading spring length of 5.3 mm and implies a linear spring force. The digital caliper measurements of the holder components are listed in Table S2.

Table S2. Cell Holder Mechanical Properties (from Part 1, see Figure 1a-b)

	Free Length (mm)	Loaded Length (mm)	ΔL (mm)
Pouch Cell	5.8	5.3	0.5
Spring	12.7	8.55	4.15
Transducer	22.0	22.0	0
Holder Channel	66.5	66.5	0

The compressive stack pressure of the transducers acting on the pouch cell can be calculated from Equation 1.

$$P = 2F/A = 2k(L_{s0}-L_s)/A_0 \qquad \text{Equation 1}$$

The area of the transducers is known to be $A_0 = 85.0\ mm^2$, and the spring constant is k = 18 lb./in from the manufacturer suggested datasheet. The inner length of the holder was measured to be 66.5 mm, and the incompressible transducers are 22.0 mm in length. The length of each spring is then calculated to be:

$$L_s = L_{ch} - 2L_T - L_B/2 \qquad \text{Equation 2}$$

From these measurements and Equation 2, the compressive stack pressure can then be estimated as in Equation 1 and plotted vs charge passed and time. The estimated ~300 kPa stack pressure of the full cell is comparable to other studies by Cannarella and Arnold, who reported a full cell stress to fluctuate between 0-600 kPa in the initial 100 cycles of a C/2 charge rate.

The estimated stack pressure of the pouch cell over the full duration of cycling initially increases rapidly and then reaches a steady state. This initial rise is insignificant for the 1C rate, but more significant for the 2C and 3C rates.

Supplementary Figures:

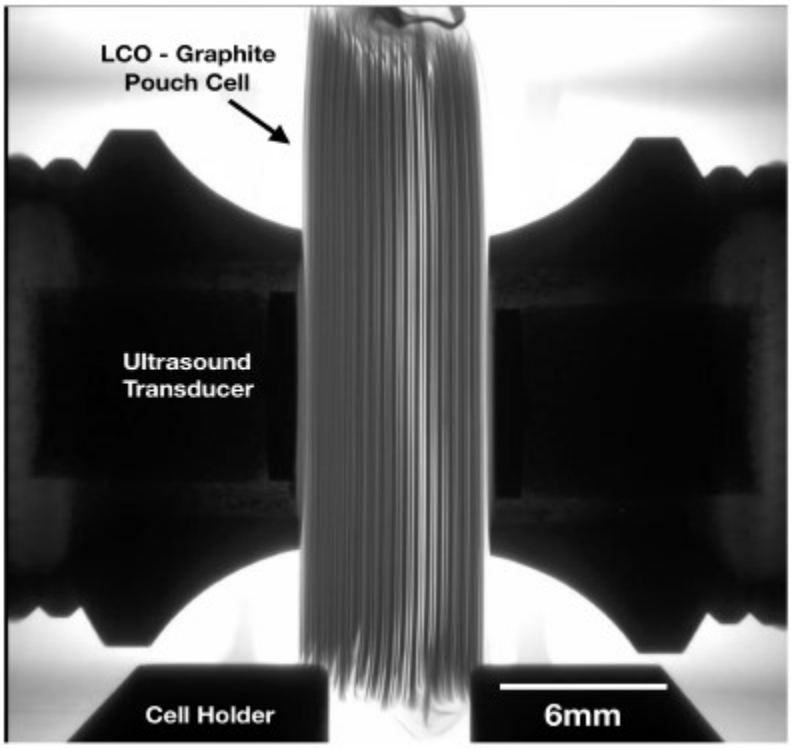

Figure S1. Transmission X-ray radiograph of the entire field of view of the $LiCoO_2$/graphite pouch cell. Transducers are on either side of the cell. Pixel variations are due to slight misalignment of some cell layers.

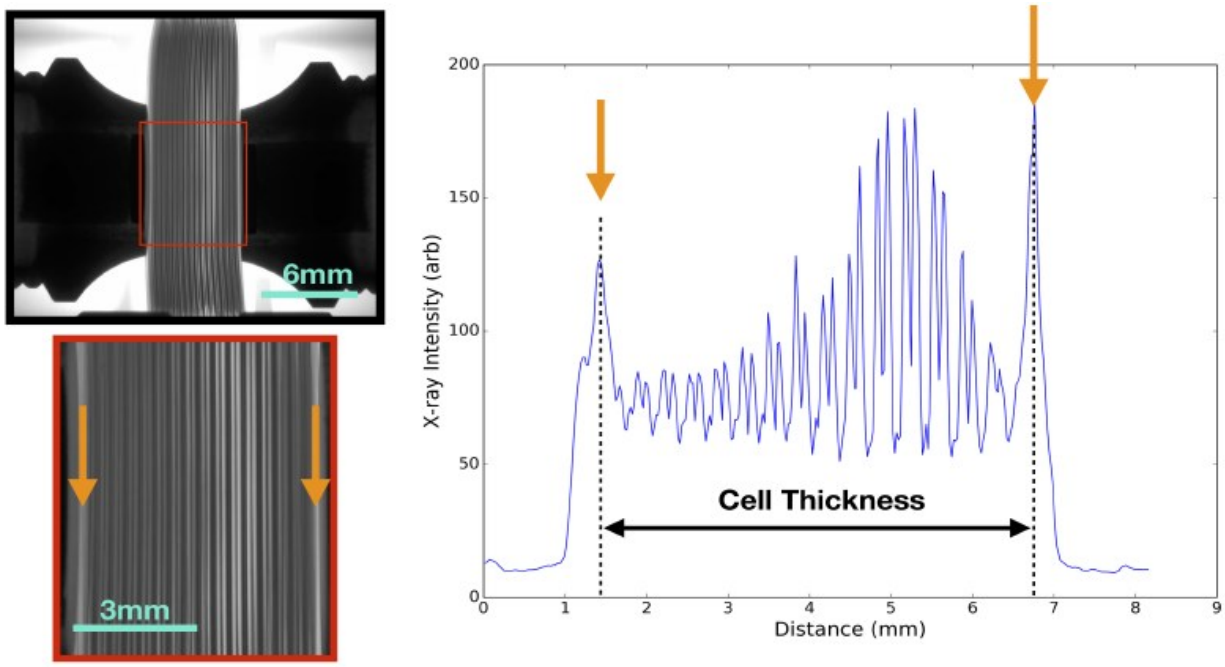

Figure S2. Depiction of method for cell thickness calculation. Pixel intensity was measured and plotted, and the maximum pixel intensities on either end were chosen to determine the total cell thickness.

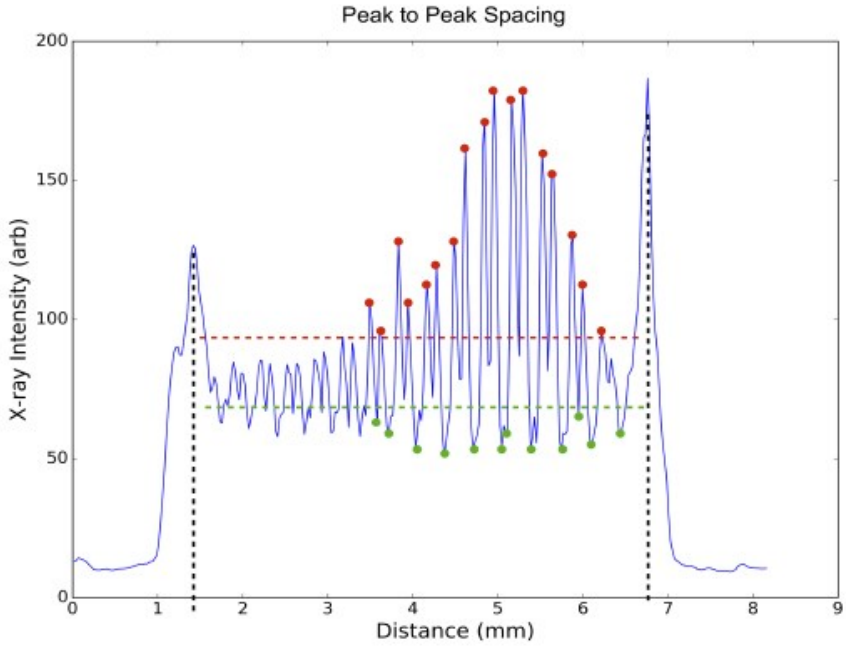

Figure S3. Individual cell layer thicknesses were calculated by taking the average peak to peak distance. A threshold was used to improve accuracy (red and green horizontal dotted lines). Red high intensity peaks correspond to the $LiCoO_2$/Al electrodes, and the green low intensity peaks correspond to the graphite/Cu electrodes.

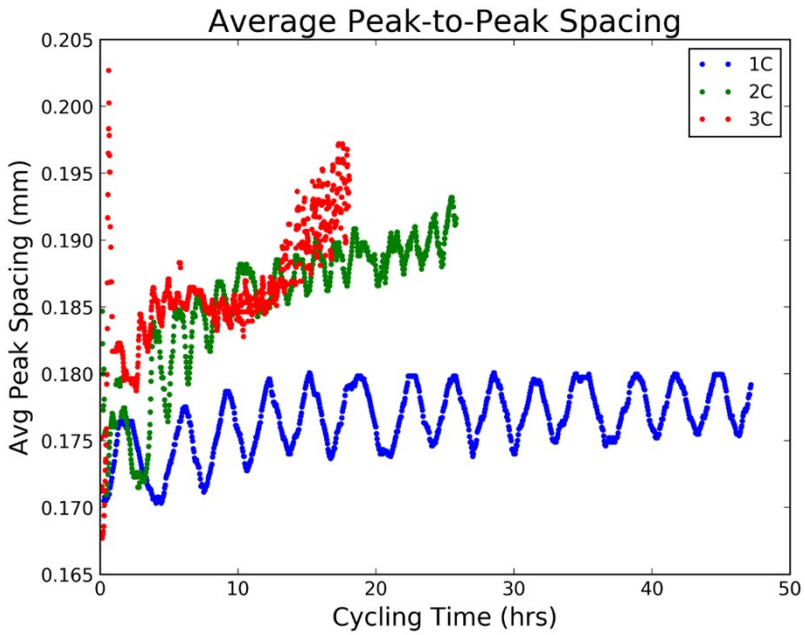

Figure S4. Average peak-to-peak spacing for approximation of average individual layer thickness (see Figure 1 for schematic of layer configuration).

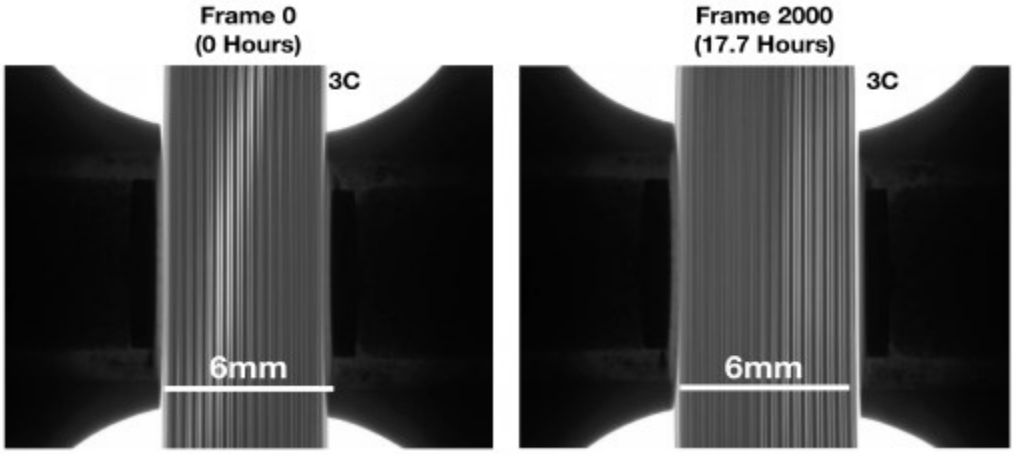

Figure S5. TXM profiles of the 3C rate cycled pouch cell before and after charge. The mechanical expansion and increased thickness is noticeable. Uneven expansion results in variations in pixel intensity before and after (note the bright region which shifts from the left side to the right side of the cell).

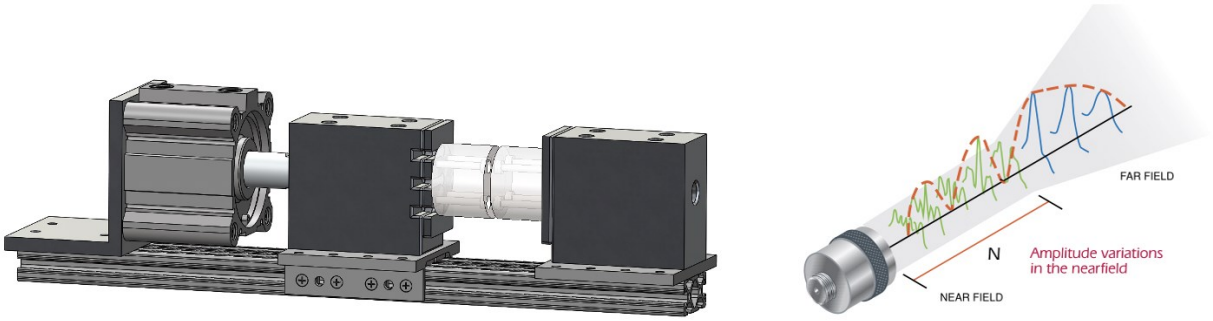

Figure S6. Design of pressure holder used for accurate acoustic measurements in a constant pressure and constant temperature environment. Pouch cell goes in between the two cylindrical Rexolite blocks which act as acoustic spacers. Depiction of near field and far field effects shows the importance of keeping the designated medium at a distance away from the transducer surface to improve signal-to-noise ratio [1].

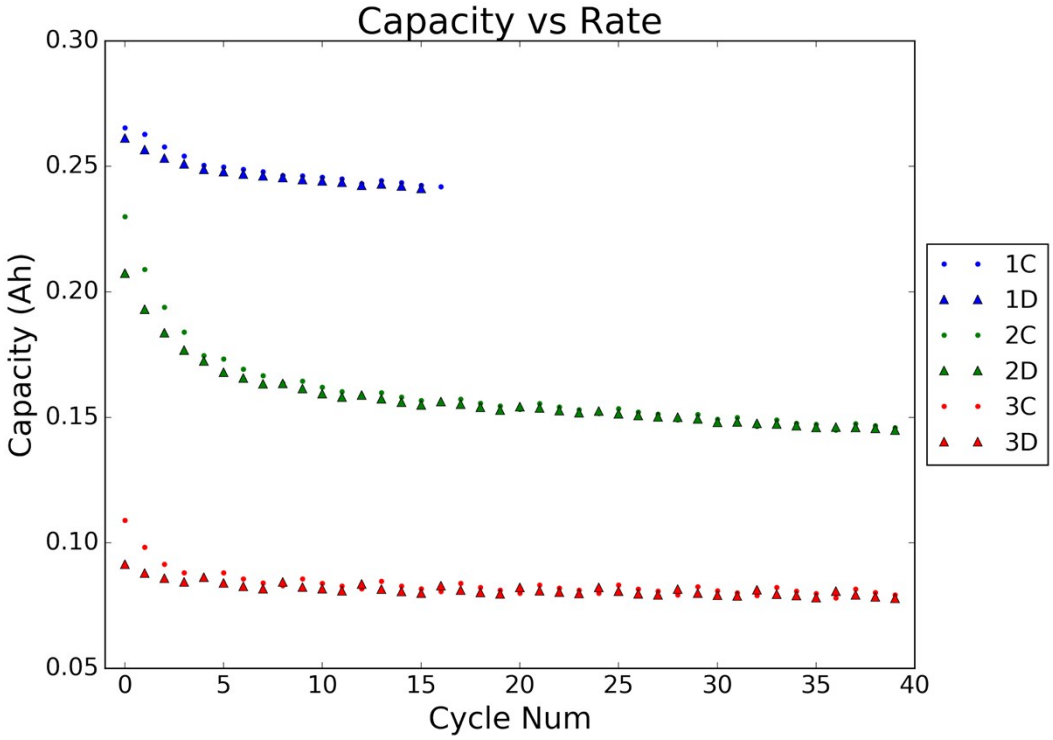

Figure S7. Capacity vs cycle number of 210 mAh $LiCoO_2$/graphite pouch cell for 1C (blue), 2C (green), and 3C (red) rates.

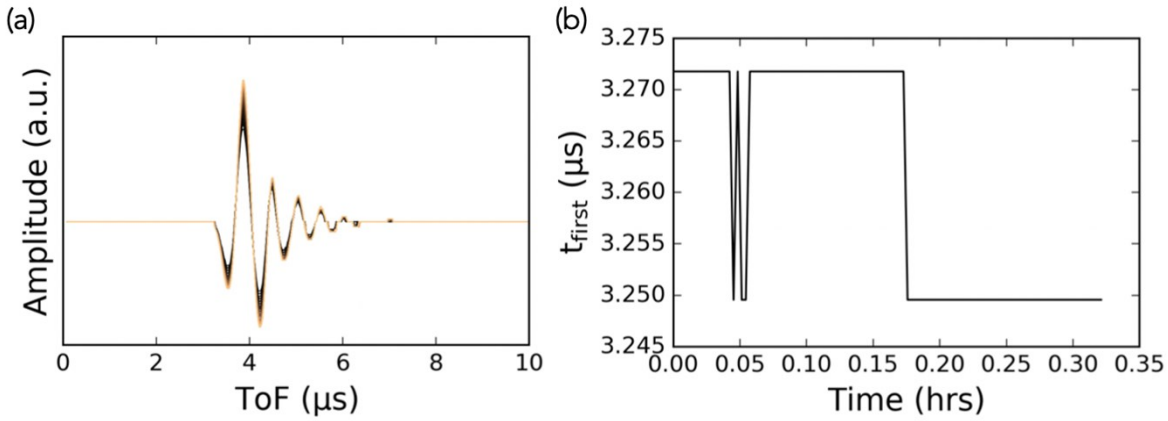

Figure S8. (a) Acoustic waveform and (b) first break for commercial acoustic pulser/receiver. Limitations in sampling time (450 points regardless of range measured) and other sources of error due to internal filtering/smoothing results in relatively poor resolution of greater than 20 ns. In comparison, Figure 2 shows that the decoupled pulser/receiver improves the resolution to less than 2 ns, resulting in improved accuracy of wave velocity and modulus measurements.

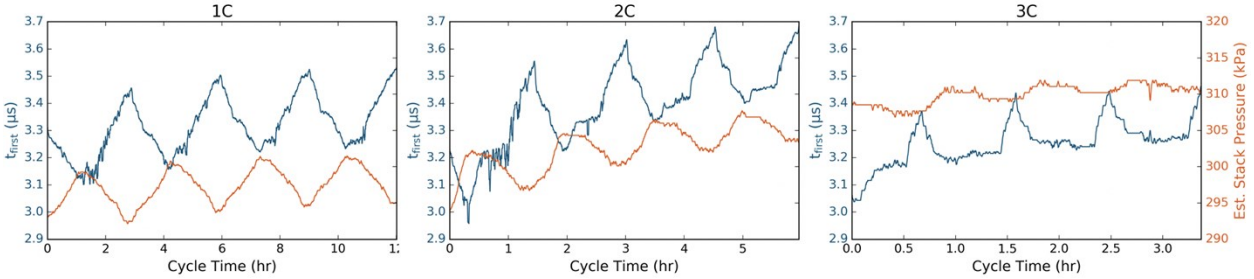

Figure S9. Estimated stack pressure (kPa) of the pouch cell placed in the spring-loaded holder and held by transducers, within the low stack pressure regime (50 kPa to 500 kPa) described by Cannarella et al. [2]

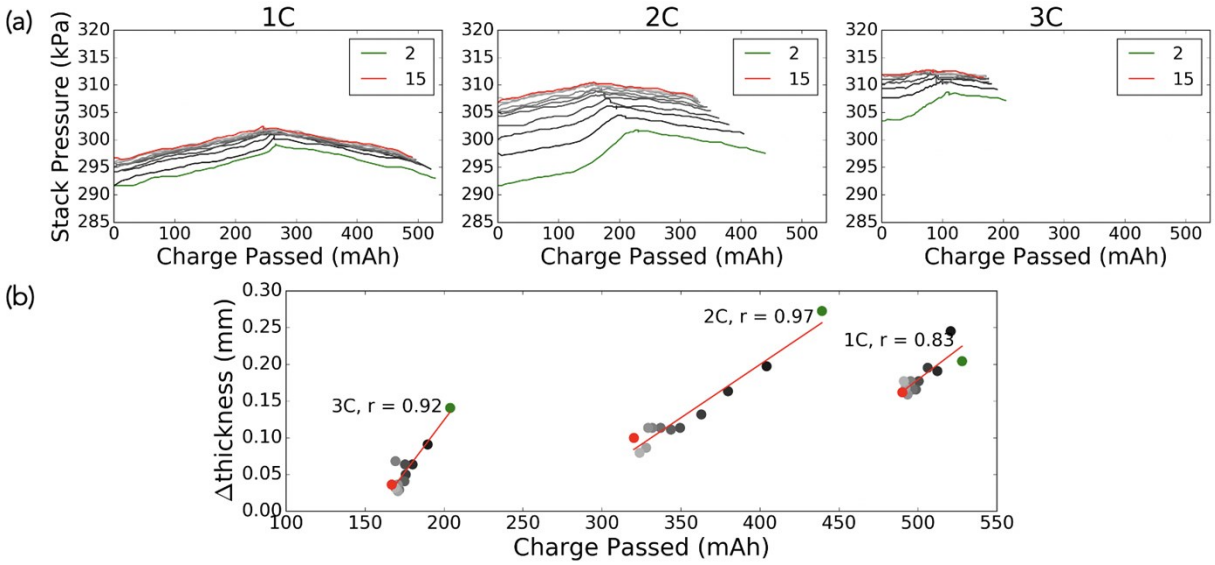

Figure S10. (a) Estimated stack pressure (kPa) of the 1C, 2C and 3C rate cells as a function of total charge passed for each cycle (mAh), and (b) peak-to-peak thickness changes as a function of charge passed (mAh) for each cycle. Green indicates cycle 2, red indicates cycle 15, with cycles in between shown by increasing color transparency.

[1] T.L. Szabo, Diagnostic Ultrasound Imaging: Inside Out, Academic Press, 2004.

[2] J. Cannarella, C.B. Arnold, Stress evolution and capacity fade in constrained lithium-ion pouch cells, J. Power Sources. 245 (2014) 745–751. https://doi.org/10.1016/j.jpowsour.2013.06.165.